ELSEVIER

Roll waves in falling films: an approximate treatment of the velocity field

Vikas Patnaik and Horacio Perez-Blanco
Department of Mechanical Engineering, The Pennsylvania State University, University Park, PA, USA

Wavy flows, an important aspect of falling film absorption in refrigeration systems, are difficult to describe analytically because of their transitional regime. Within the wavy-laminar flow regime, high-frequency capillary waves are known to exist below a Reynolds (Re) number of 200. Above the critical Re, inertial waves driven by gravity, known as roll waves, can exist. These low-frequency waves, observed in an experimental absorber, were identified via image-processing studies of the falling film. A frequency analysis (fast Fourier transformation — FFT) of the film thickness trace in time yielded a wave frequency corresponding to roll waves at the given Re. A hydrodynamic description of this flow regime was then obtained from the literature. The flow equations provided by this model were solved for various wave parameters at different Reynolds numbers. The results from the solution were then extended using Fourier series expansions and continuity at each point to yield the complete periodic velocity field.

Introduction

The design of many heat exchangers incorporates falling films. In large tonnage absorption machines, falling film absorbers are frequently used. Vertical tube absorbers are used to gain a basic understanding of the flow and heat and mass transfer phenomena associated with falling films (Patnaik 1994). Understanding the complex falling film hydrodynamics is necessary for the prediction of absorber performance. However, wavy falling in transitional regime are difficult to model.

The hydrodynamics of falling films has been studied by numerous researchers (Kapitza 1948; Tailby and Portalski 1960; Levich 1962; Massott et al. 1966). However, in most cases, the theoretical and experimental results are not in good agreement. The cause of the discrepancy is probably the inadequate modeling of waves. Hydrodynamic studies indicate that film flows can be broadly categorized into three regimes (Grossman 1984), depending on the film Reynolds number, defined as follows:

$$\mathrm{Re}_s = 4\ \mathrm{Re} = 4\Gamma/\mu = 4\bar{w}\bar{\delta}/\nu \qquad (1)$$

The regimes are:
(1) the smooth laminar flow, for $\mathrm{Re}_s \leqslant 20$;
(2) flow with surface waves, of partially laminar and partially turbulent nature, in $20 < \mathrm{Re}_s < 4000$; and
(3) fully turbulent flow, for $\mathrm{Re}_s \geqslant 4000$.

In the wavy flow regime (2), transition to turbulence and the surface disturbances become more significant with increasing Reynolds number. This transition regime can then be subdivided into capillary wavy–laminar, inertial wavy–laminar, and inertial wavy–turbulent flow regimes, corresponding approximately to the Reynolds number ranges, $20 < \mathrm{Re}_s < 200$, $200 < \mathrm{Re}_s < 1000$, and $1000 < \mathrm{Re}_s < 4000$, respectively. The inertial waves are known as "roll" waves, because of their appearance of rolling down over a film substrate.

In the low Reynolds number range of $20 < \mathrm{Re}_s < 200$, surface tension forces play a key role in the manifestation of the waves. These forces appear as consequence of localized temperature and concentration gradients and become important when their magnitude is comparable to that of the gravity and viscous forces. The capillary waves appear as ripples on the film surface, being of high frequency and small amplitude. Based on Kapitza's pioneering work, Levich (1962) presented a theoretical analysis of this wavy flow regime, resulting on sinusoidal traveling waves, as shown in Figure 1a. The analysis is however, limited to waves of small amplitude and wavelength at least 13.7 times larger than the film thickness. Improved capillary-wave hydrodynamic solutions followed Kapitza's model, such as the solutions of Penev et al. (1972) and Barrdahl (1986). Using dynamic singularity theory, Chang (1987) derived closed-form solutions for the evolution of these finite amplitude waves. Other low Re solutions to the Navier–Stokes equations, using finite-element methods, have been obtained to study wave development from initial perturbations on the smooth film (Bach and Villadsen 1984; Kheshgi and Scriven 1987).

Roll waves are governed by the interplay of inertia (attributable to the higher Reynolds numbers) and gravity, with surface tension effects becoming negligible in comparison. These waves have longer wavelengths and much lower frequencies than capillary waves. The roll wave regime has been studied via numerical methods (Wasden and Dukler 1989). More recent analyses specify the velocity distribution and wave parameters more accurately in terms of the flow conditions (Brauner 1989). The waves occur at Reynolds numbers ranging from 200 to 4000 (Figure 1b), and tend to overtake the smaller, capillary waves, resulting in a complicated surface structure that appears to be *random* in nature. Experimental studies have shown that, under constant operating conditions, roll waves travel with an almost constant

Address reprint requests to Prof. H. Perez-Blanco, Department of Mechanical Engineering, The Pennsylvania State University, University Park, PA 16802, USA.

Received 20 January 1995; accepted 23 August 1995

Int. J. Heat and Fluid Flow 63–70, 1996

655 Avenue of the Americas, New York, NY 10010

0142-727X/96/$15.00
SSDI 0142-727X(95)00075-5

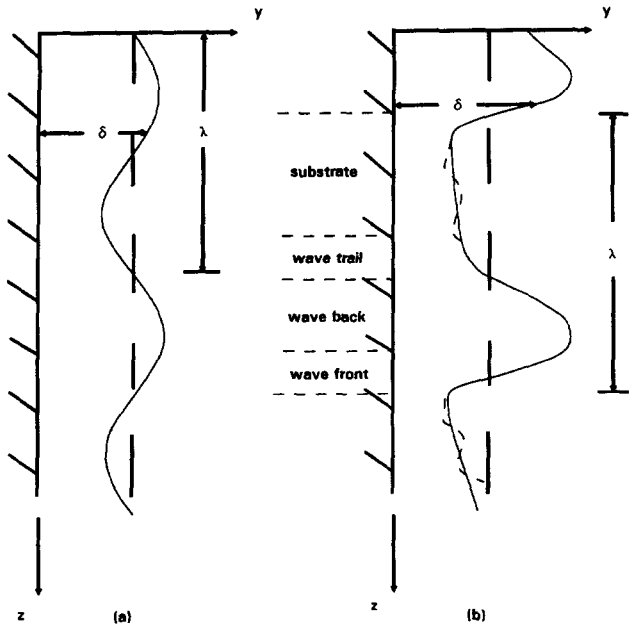

Figure 1 (a) capillary waves; (b) roll waves

celerity (wave velocity normalized with respect to average fluid velocity) and can be identified quite easily over a wide range of Reynolds numbers (Karapantsios and Karabelas 1990).

Roll waves have also been known to be induced artificially at lower Reynolds numbers, via a pulsating liquid flow (Miller et al. 1992). In the course of Miller's experiments, low-frequency *roll* waves were observed in the film at low Re numbers, in the order of 100. The occurrence of the waves coincided with enhancement of the absorption rates. The waves are believed to be the cause of the enhanced absorption with respect to the *capillary* wavy-laminar model predictions (Patnaik et al. 1993).

The objective of this work is to gain an understanding of the velocity field associated with the roll waves. Such an understanding allows the solution of the governing heat and mass transport equations for falling-film absorption. Hence, a comprehensive model to explain the absorption enhancement by roll waves becomes possible once the velocity field is known. Image-processing techniques together with wave relationships extracted from the literature are used to determine the velocity field.

Table 1 Fluid properties

Fluid	Density kg/m^3	Viscosity cP	Surface tension, N/m
Water	998	1	0.0725
60% LiBr	1712	10	0.0918

* All quantities in S.I. units.

Image processing

Video recordings of the falling film over vertical tubes of various diameters were obtained (Miller 1992). The camera was placed at different locations along the length of the tube. Tap water and aqueous lithium bromide solution (60% by weight) were filmed at a temperature of 74°F. Table 1 lists relevant properties (Uemura and Hasaba 1964).

A standard image-processing system was employed to characterize the wavy flow (Patnaik 1994). Given the film Reynolds number, wave parameters such as amplitude, frequency, and celerity can be determined. Film thickness was the basis for determination of wave parameters. For a known flow rate, the thickness was measured at a fixed location, for seven randomly chosen video frames. The average thickness, crest, and trough for the different tube diameters and fluids are shown versus Reynolds number in Figures 2 and 3. In Figure 2 for water flowing over a 3/4-in. tube, the waves are of slightly smaller amplitude near the top of the tube, particularly between Re_s of 800 and 1000. This is possibly because of the developing nature of the flow here. The amplitude increases with Reynolds number at both locations, although there is a dampening above $Re_s \cong 960$ at the downstream location. This Reynolds number nearly marks the transition from wavy-laminar to wavy-turbulent flow. The energy of the waves in the transition region could be diverted to changes in flow structure, causing a drop in the amplitude. The amplitude-dampening is not observed in the case of the lithium bromide solution, falling over two smaller tubes 1/2-in. and 3/8-in. in

Notation *

a_n, b_n	Fourier series coefficients
F	wave frequency
l	roll wave zone length
Re	Reynolds number
t	time
w	longitudinal velocity
v	transverse velocity
W	wave velocity
y	transverse coordinate (from outer wall)
z	longitudinal coordinate (from top)

Greek

Γ	mass flow rate per unit film width
δ	film thickness
λ	wavelength
$\xi = z - \mathrm{Wt}$	streamwise coordinate in frame of reference moving with the wave
σ	surface tension coefficient
μ	dynamic viscosity
ν	kinematic viscosity
ρ	density
$\Omega = \bar{w}\delta$	volumetric (flow) rate

Subscripts

w	wave back region
F	wave front region
if	interface
P	wave peak
s	(absorbent) solution
S	film substrate region
T	wave trail region

Superscript

$\bar{}$	average quantity

* All quantities in S.I. units.

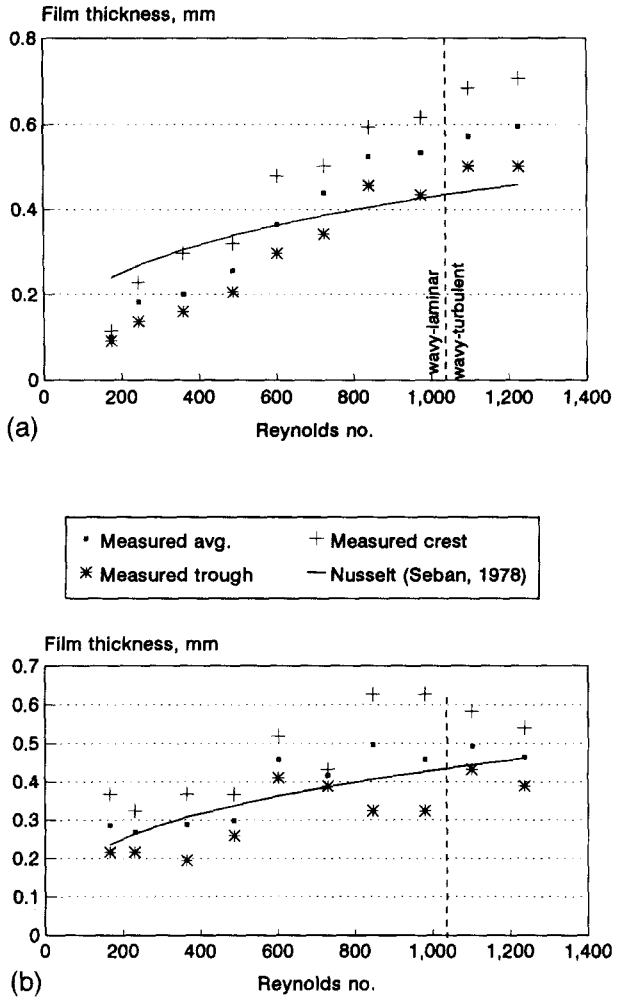

Figure 2 (a) Film thickness, crests, and troughs as functions of Reynolds number; water down 3/4-in. tube, $z = 2.5$ cm (Miller 1992); □ measured avg.; + measured crest; * measured trough; – Nusselt (Seban 1978). (b) Film thickness, crests, and troughs as functions of Reynolds number; water down 3/4-in. tube, $z = 33.5$ cm (Miller 1992); □ measured avg.; + measured crest; * measured trough; – Nusselt (Seban 1978)

diameter (Figure 3). This is because the kinematic viscosity of the 60% LiBr solution is ~ 6 times larger than that of water, so that for similar mass flow rates, transition is delayed. Also, for both tube sizes, the thickness and amplitude are measured at only 8–10 cm from the top. Both quantities appear smaller for the waves over the smaller tube. The image-processing measurements agree well with Nusselt's predictions (Seban 1978).

Frequency analysis

Wave frequency is probably the most crucial parameter defining wave type. Given the transitional nature of the flow, we would expect many frequencies to be present in the falling film signal. However, a single frequency could be dominant (that of the roll waves) and most instrumental in transport enhancement. To identify this frequency, the time-domain signal can be subjected to a Fourier transform, which would map it onto the frequency domain (Oran Brigham 1974). The most significant peak in the Fourier coefficient function would correspond to the dominant frequency of the waves. Other peaks would represent second- and higher-order wave frequencies.

The sampling rate of our system (30 frames per second) precluded identification of any dominant frequencies above ~ 15 Hz, because of aliasing (Oran Brigham 1974). However, in the flow range of interest ($200 < Re_s < 300$), roll waves occur at frequencies below 15 Hz (Brauner 1989). Each dataset consisted of 30 points, spanning over an interval of 1 second. One such interval is shown in Figure 4, for LiBr solution flowing down a 3/4-in. tube at a flow rate of 2.83 lb/min (0.02 kg/s or $Re_s = 220$); plot (a) is the film thickness signal in the time domain, and plot (b) is the FFT of this signal yielding the Fourier coefficient function in frequency domain. From Figure 4b, a dominant 13-Hz frequency and a secondary 5-Hz emerge. The 13-Hz frequency was consistently detected in three out of four other populations. Thus, amplitude and frequency analysis of the aqueous LiBr film thickness confirms the presence of relatively small roll waves in flows with $Re_s < 300$.

Hydrodynamics

An extensive search of the literature for a model for falling films with roll waves resulted on the selection of Brauner's integral

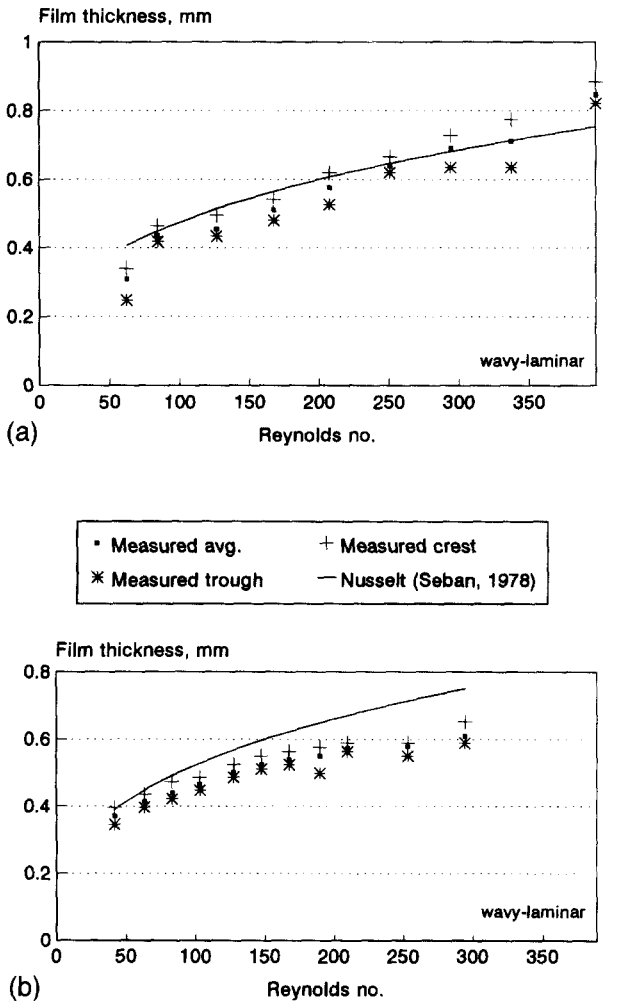

Figure 3 (a) Film thickness, crests, and troughs as functions of Reynolds number; LiBr solution down 1/2-in. tube, $z = 10$ cm (Miller 1992); □ measured avg.; + measured crest; * measured trough; – Nusselt (Seban 1978). (b) Film thickness, crest, and troughs as functions of Reynolds number; LiBr solution down 3/8-in. tube, $z = 8$ cm (data of Miller 1992); □ measured avg.; + measured crest; * measured trough; – Nusselt (Seban 1978)

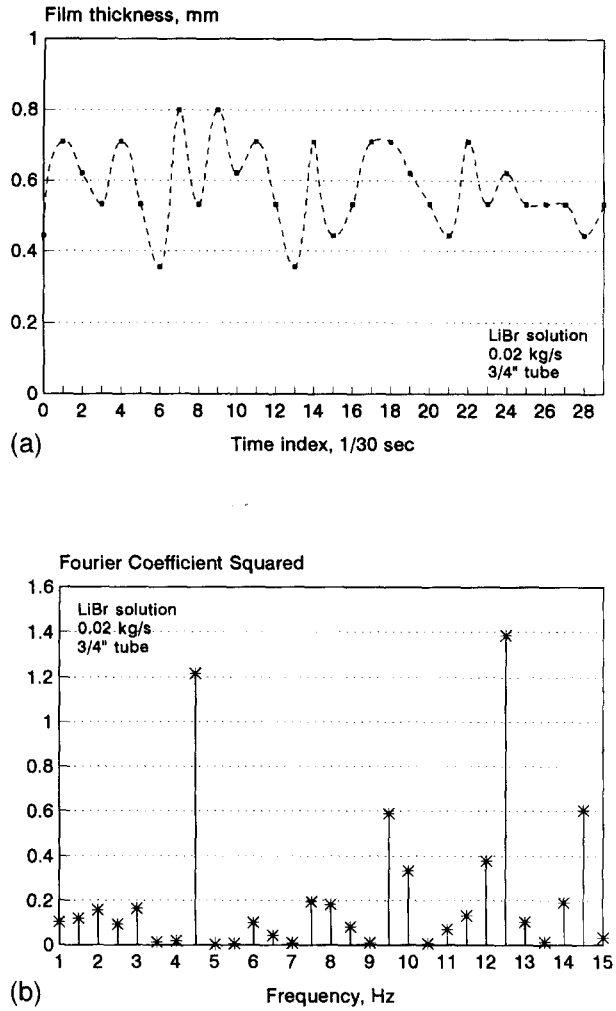

Figure 4 (a) Film thickness signal in time. (b) Falling film Fourier coefficients

solution (1989). The basis of this selection can be found in *Figure 5*, where wave frequency is plotted against film Reynolds number for two different flow situations, described in detail later.

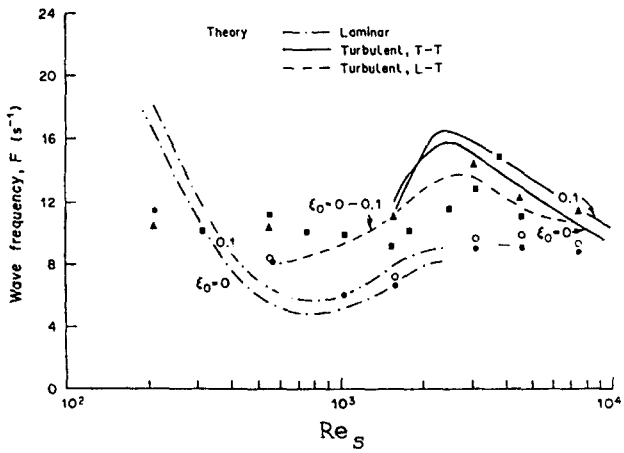

Figure 5 Roll wave frequency as a function of falling film flow, symbols indicate experimental measurements (adapted from Brauner 1989)

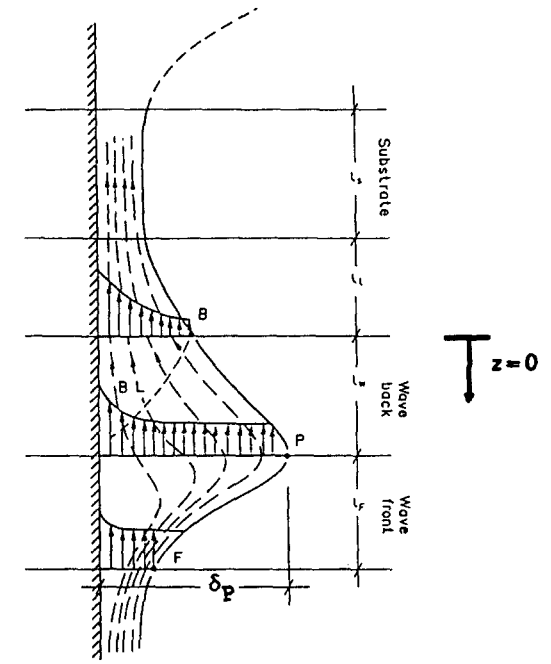

Figure 6 Schematic description of a laminar roll wave in moving coordinates (adapted from Brauner 1989)

For $Re_s = 220$, the wave frequency is between 14 and 16 Hz, which is reasonably close to our image-processing result.

Transport enhancement attributable to waves is due to the convective effect of the transverse velocity component absent in smooth films (Ruckenstein and Berbente 1965). The magnitude of this component depends on the wave frequency and phase relations with the streamwise component and appears to be independent of film thickness.

Brauner's model (1989) is based on the fact that different mechanisms control the flow in the various zones along a roll wave. The solution of the model equations pertaining to each zone yields the velocity, film thickness, and wave parameters at the zone boundaries. Reasonably satisfactory agreement between the theoretical predictions and experimental data was obtained over a wide range of film Re. Hence, this hydrodynamics is an adequate input to the absorption model.

In *Figure 6*, a moving coordinate system, defined by the transformation:

$$\xi = z - Wt \tag{2}$$

attaches the frame of reference to a wave traveling down at speed W, so that the stationary tube wall now appears to move upward at the same speed. The existence of a maximum-velocity point at the wave back and a minimum-velocity point at the wave front along the interface corresponds to gradual changes in the velocity field within the wave and relatively low velocities at the wave peak. This is the inertial wavy-laminar flow regime, which typically occurs at $Re_s < 1000$, where a inertial wavy–laminar flow regime, which typically occurs at $Re_s < 1000$, where a laminar-substrate *laminar*-wave back situation prevails. This regime corresponds well to the relatively low Reynolds numbers for absorbent flow ($Re_s \geq 200$).

The formulation of the continuity and momentum equations for the wave front, wave back, and substrate yields 12 nonlinear, algebraic equations in twelve unknowns, with the wave velocity a function of Re as given by Brauner (1989) (l_F, δ_P, $\overline{w}_P$, l_w, δ_w, $\overline{w}_w$, l_T, l_S, δ_S, $\overline{w}_S$, Ω, F, and W). The equations were solved for the constant-celerity or "equilibrium" region, *at least* ~ 1-m downstream of the injection point (Aragaki et al. 1987). The solution scheme was the iterative Levenberg–Marquardt method.

Film thickness and velocity field

Brauner's (1989) formulation yields the length, the film thickness, and the *average* velocity at each wave zone. However, the film thickness and average velocity are calculated only at three locations (demarcating the zones) along the length of the wave. Also, only information on the streamwise velocity is obtained; the transverse component, postulated to play a crucial role in absorption enhancement due to waves, remains unknown. Hence, after solving Brauner's equations, three tasks remain to be performed: (1) the selection of a suitable velocity profile, given the average velocity at each station; (2) the introduction of periodicity along the entire length of the absorber, so that, whenever a wave passes through a given location, the falling film thickness assumes the calculated values at the three stations of the wave; and (3) the derivation of the transverse velocity component.

Our assumption of streamlined fluid flow within the wave; i.e., laminar-substrate and -wave back, allows us to use a parabolic velocity profile in each zone. The transverse variation in streamwise velocity is given by:

$$w(t, y, z) = 1.5\ \bar{w}(t, z)\left[2\frac{y}{\delta(t, z)} - \left(\frac{y}{\delta(t, z)}\right)^2\right] \tag{3}$$

where appropriate functions for the space–time periodicity of the film thickness and average velocity still need to be derived.

The following film thickness function in can then be constructed as a linear approximation:

$$\delta = \delta_S, \qquad \frac{\lambda}{2} \le z < -l_T$$

$$\delta = \frac{\delta_W - \delta_S}{l_T} z + \delta_W, \qquad -l_T \le z < 0$$

$$\delta = \frac{\delta_P - \delta_W}{l_W} z + \delta_W, \qquad 0 \le z < l_W$$

$$\delta = \frac{\delta_S - \delta_P}{l_F}(z - l_W) + \delta_P, \qquad l_w \le z < (l_w + l_F)$$

$$\delta = \delta_S, \qquad (l_w + l_F) \le z < \frac{\lambda}{2} \tag{4}$$

[The average velocity function can be constructed in the same manner, over the interval $(\lambda/2, \lambda/2)$]. A smooth function, periodic in space–time and passing through the known points, was obtained with a three-term Fourier series as follows:

$$\delta(z) = a_0 + \sum_{n=1}^{3}\left[a_n \cos\left(\frac{2n\pi z}{\lambda}\right) + b_n \sin\left(\frac{2n\pi z}{\lambda}\right)\right] \tag{5}$$

where the coefficients a_0, a_n, and b_n are given in the Appendix. (A similar function was derived for $\bar{w}(z)$, obtained by replacing $\delta_{S,w,P}$ in the Fourier coefficients by $\bar{w}_{S,w,P}$, respectively). Higher-order Fourier series yielded progressively coarser profiles. Finally, the nonstationarity of the waves was introduced by replacing the streamwise coordinate z by ξ, where, as defined before, ξ is the "moving" streamwise coordinate.

The transverse velocity component was derived using the two-dimensional (2-D) continuity equation for an incompressible fluid:

$$\frac{\partial w}{\partial z} + \frac{\partial v}{\partial y} = 0 \tag{6}$$

$$\therefore\ v = -\int \frac{\partial w}{\partial z}\, dy + (\text{function of z}) \tag{7}$$

Now, differentiating Equation 3 partially with respect to z, we have the following:

$$\frac{\partial w}{\partial z} = 1.5\left\{\bar{w}(t, z)\left[-\frac{2y}{\delta^2(t, z)} + \frac{2y^2}{\delta^3(t, z)}\right]\frac{\partial \delta}{\partial z} + \frac{\partial \bar{w}}{\partial z}\left[\frac{2y}{\delta(t, z)} - \left(\frac{y}{\delta(t, z)}\right)^2\right]\right\} \tag{8}$$

where $\bar{w}(t, z)$ and $\delta(t, z)$ are the functions obtained with the Fourier series expansion. Substituting Equation 8 in Equation 7 and integrating, we get the following:

$$v = -1.5\left[\bar{w}\left(\frac{2y^2}{2\delta^2} + \frac{2y^3}{3\delta^3}\right)\frac{\partial \delta}{\partial z} + \frac{\partial \bar{w}}{\partial z}\left(\frac{2y^2}{2\delta} - \frac{y^3}{3\delta^2}\right)\right] + (\text{function of } z) \tag{9}$$

$$\text{i.e.} \quad v(t, y, z) = 1.5\left\{\bar{w}\frac{\partial \delta}{\partial z}\left[\left(\frac{y}{\delta}\right)^2 - \frac{2}{3}\left(\frac{y}{\delta}\right)^3\right] - \frac{\partial \bar{w}}{\partial z}\delta\left[\left(\frac{y}{\delta}\right)^2 - \frac{1}{3}\left(\frac{y}{\delta}\right)^3\right]\right\} + (\text{function of } z) \tag{10}$$

Applying the no-transpiration boundary condition all along the tube wall to this solution, we have: At $y = 0$, $v = 0 + (\text{function of } z)$, which means that the function of z is zero. Thus, the transverse velocity component assumes the following form:

$$v(t, y, z) = 1.5\left\{\bar{w}\frac{\partial \delta}{\partial z}\left[\left(\frac{y}{\delta}\right)^2 - \frac{2}{3}\left(\frac{y}{\delta}\right)^3\right] - \frac{\partial \bar{w}}{\partial z}\delta\left[\left(\frac{y}{\delta}\right)^2 - \frac{1}{3}\left(\frac{y}{\delta}\right)^3\right]\right\} \tag{11}$$

and the hydrodynamics of roll waves is fully described and ready for input to the governing equations of the heat and mass transfer problem.

Results from the above interpretation of Brauner's (1989) work on roll waves have been summarized in Figures 7–14, for a film Reynolds number of 400. In Figures 7 and 8, the film thickness has been plotted in the time and space (z-) domains,

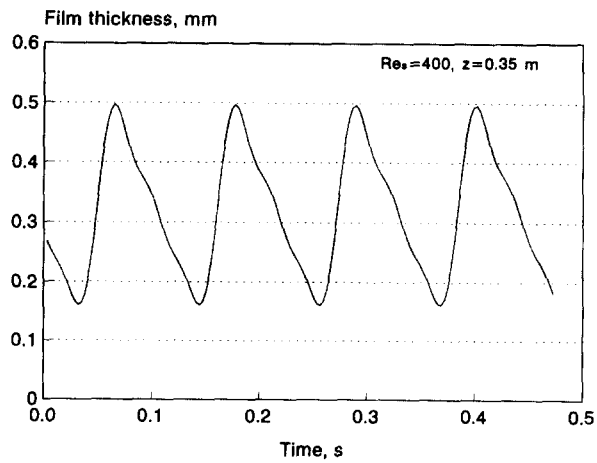

Figure 7 Wavy film hydrodynamics: film thickness as a function of time

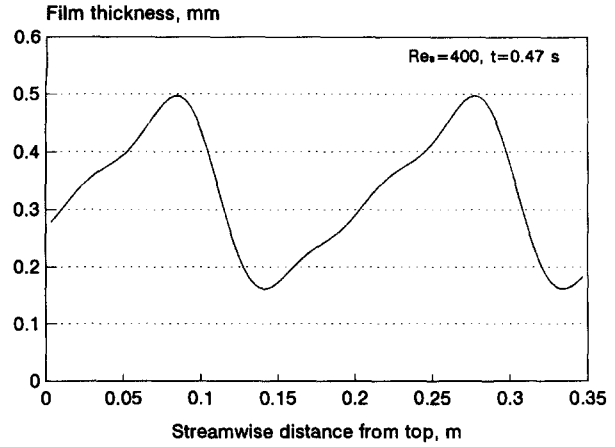

Figure 8 Wavy film hydrodynamics: film thickness as a function of vertical position

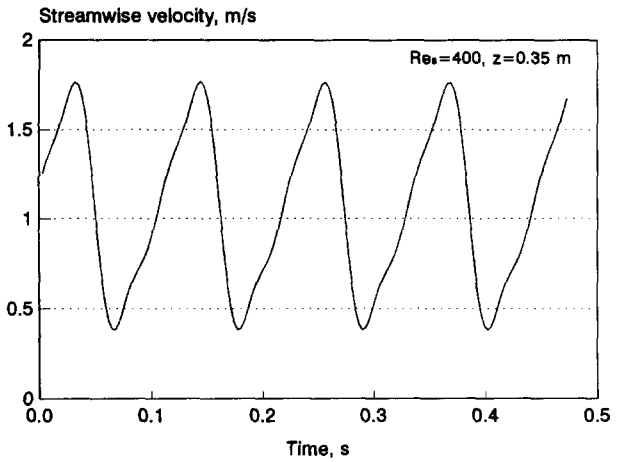

Figure 9 Wavy film hydrodynamics: bulk streamwise velocity as a function of time

respectively. Figures 9 and 10 show the average streamwise velocity in the two domains. The average transverse velocity can be positive or negative, depending on the phase of the wave passing through the point or instant of interest, as shown in Figures 11 and 12. Owing to the asymmetrical profile of the

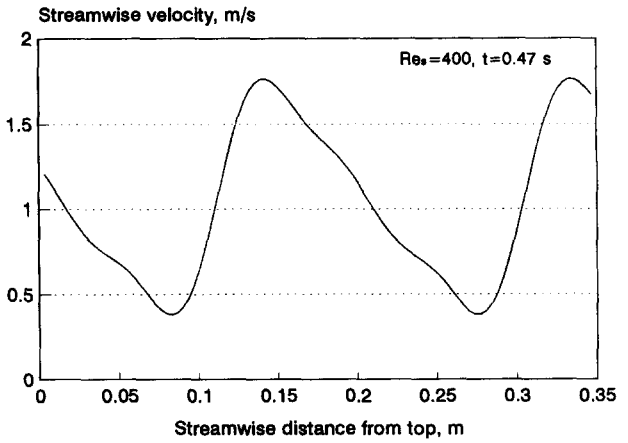

Figure 10 Wavy film hydrodynamics: bulk streamwise velocity as function of vertical position

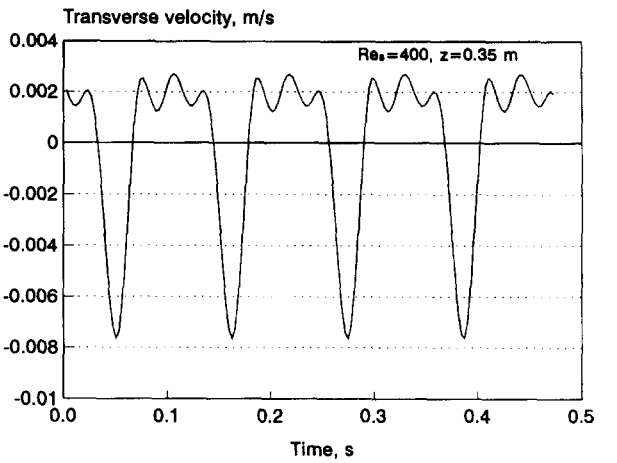

Figure 11 Wavy film hydrodynamics: bulk transverse velocity as a function of time

inertia–gravity-driven roll wave, the incoming phase of this velocity component is larger in magnitude and lesser in spread than the outgoing phase. The resulting significant normal convection, in conjunction with the crests in streamwise convection (Figures 9 and 10), has been postulated to be the cause for transport enhancement in falling films with roll waves (Patnaik 1994). Velocity profiles at different instants are shown in Figures 13 and 14.

Conclusions

This work presents a study of the hydrodynamics of falling films. Various flow regimes have been identified, based on ranges of the film Reynolds number.

Under typical operating conditions of vertical tube absorbers, roll waves were observed to occur in the film at Reynolds numbers over 200. These waves enhance the transport processes significantly, primarily through convection. An image-processing system was developed to identify and study these waves in detail. An outcome of this study is the relationship between wave parameters and flow parameters. Thus, roll waves with a frequency of approximately 13 Hz were observed in a film flowing with a Reynolds number of 220.

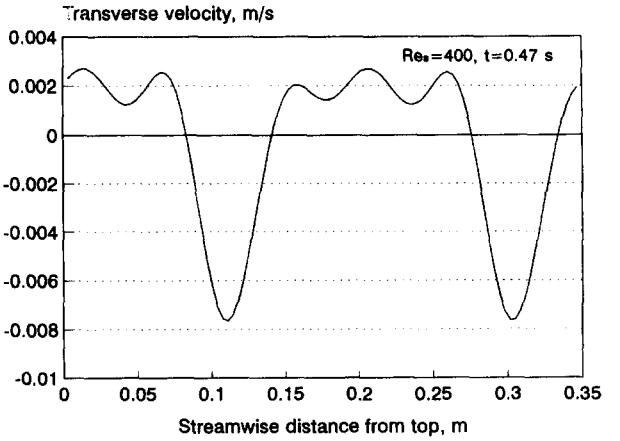

Figure 12 Film hydrodynamics: bulk transverse velocity as function of vertical position

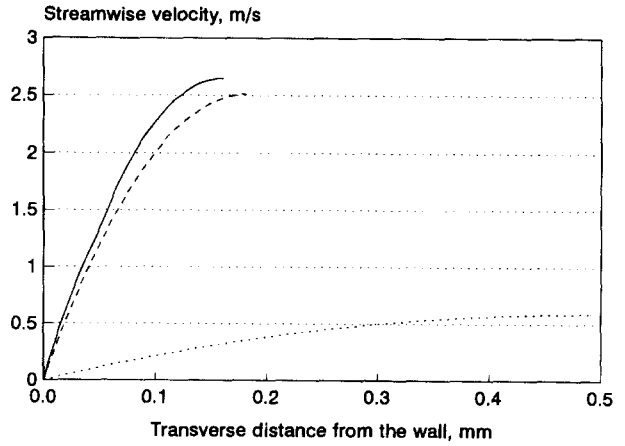

Figure 13 Streamwise velocity profiles at different times; $Re_s = 400$, $z = 0.35$ m; ——— $t = 0.15$ s; $t = 0.3$ s; ----- $t = 0.47$ s

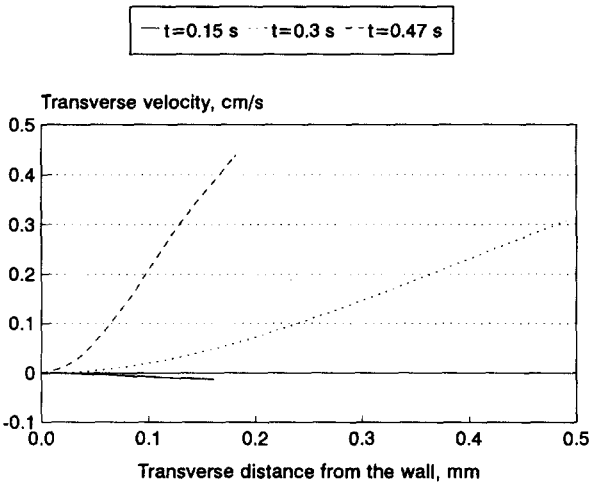

Figure 14 Transverse velocity profiles at different times; $Re_s = 400$, $z = 0.35$ m; ——— $t = 0.15$ s; ····· $t = 0.3$ s; ----- $t = 0.47$ s

A model from the literature was adopted to formulate the falling-film velocity field. This velocity field could then serve as input to the governing partial differential equations of species and thermal transport that describe the absorption process.

Attempts to predict mass transfer enhancement attributable to waves require a realistic estimation of the transverse velocity component (Wasden and Dukler 1990). The present work, provides such an estimate. The explicit algebraic expressions for the velocity field derived here readily allow for the numerical solution of the energy and species transport. Hence, an evaluation of transport enhancement caused by waves becomes possible.

Acknowledgments

The authors would like to thank Mr. William Ryan of the Gas Research Institute for funding part of this work and Mr. William Miller of Oak Ridge National Laboratory for his collaboration through the video filming of the falling films for image processing.

Appendix

The Fourier series coefficients derived for the film thickness and average velocity functions are given by:

$$a_0 = \frac{1}{\lambda}\int_{-\lambda/2}^{\lambda/2} \delta(z)\,dz$$

$$= \frac{1}{\lambda}\left[\delta_S\left(\lambda - \frac{l_T}{2} - l_w - \frac{l_F}{2}\right) + \frac{\delta_w}{2}(l_T + l_w) + \frac{\delta_P}{2}(l_w + l_F)\right] \tag{A1}$$

$$a_n = \frac{2}{\lambda}\int_{-\lambda/2}^{\lambda/2} \delta(z)\cos\left(\frac{2n\pi z}{\lambda}\right)dz$$

$$= (\delta_w - \delta_S)\left(\frac{1}{n\pi}\sin\left(\frac{2n\pi l_T}{\lambda}\right)\right.$$

$$+ \frac{1}{l_T}\left[\frac{\lambda}{2(n\pi)^2}\left[1 - \cos\left(\frac{2n\pi l_T}{\lambda}\right)\right]\right.$$

$$\left.\left. - \frac{l_T}{n\pi}\sin\left(\frac{2n\pi l_T}{\lambda}\right)\right]\right) + \frac{\delta_P\delta_w}{l_w}\left\{\frac{\lambda}{2(n\pi)^2}\right.$$

$$\times\left[\cos\left(\frac{2n\pi l_w}{\lambda}\right) - 1\right] + \frac{l_w}{n\pi}\sin\left(\frac{2n\pi l_T}{\lambda}\right)\Bigg\}$$

$$+ \frac{\delta_w}{n\pi}\sin\left(\frac{2n\pi l_w}{\lambda}\right) + \frac{\delta_S\delta_P}{l_F}\left\{\frac{\lambda}{2(n\pi)^2}\right.$$

$$\times\left[\cos\left(\frac{2n\pi l_S}{\lambda}\right) - \cos\left(\frac{2n\pi l_w}{\lambda}\right)\right]$$

$$\left.+ \frac{1}{n\pi}\left[(l_w + l_F)\sin\left(\frac{2n\pi l_S}{\lambda}\right) - l_w\sin\left(\frac{2n\pi l_w}{\lambda}\right)\right]\right\}$$

$$+ \frac{\delta_P - l_w/l_F(\delta_S - \delta_P)}{n\pi}\left[\sin\left(\frac{2n\pi l_S}{\lambda}\right)\right.$$

$$\left. - \sin\left(\frac{2n\pi l_w}{\lambda}\right)\right] + \frac{\delta_S}{n\pi}\sin\left(\frac{2n\pi l_S}{\lambda}\right) \tag{A2}$$

$$b_n = \frac{2}{\lambda}\int_{-\lambda/2}^{\lambda/2} \delta(z)\sin\left(\frac{2n\pi z}{\lambda}\right)dz$$

$$= -\frac{\delta_S}{n\pi}\left[\cos\left(\frac{2n\pi l_T}{\lambda}\right)\cos\left(\frac{2n\pi l_S}{\lambda}\right)\right]$$

$$+ \frac{\delta_w - \delta_S}{l_T}\left[\frac{\lambda}{2(n\pi)^2}\sin\left(\frac{2n\pi l_T}{\lambda}\right) - \frac{l_T}{n\pi}\cos\left(\frac{2n\pi l_T}{\lambda}\right)\right]$$

$$- \frac{\delta_w}{n\pi}\left[1 - \cos\left(\frac{2n\pi l_T}{\lambda}\right)\right]$$

$$+ \frac{\delta_P - \delta_w}{l_w}\left[\frac{\lambda}{2(n\pi)^2}\sin\left(\frac{2n\pi l_w}{\lambda}\right) - \frac{l_w}{n\pi}\cos\left(\frac{2n\pi l_w}{\lambda}\right)\right]$$

$$- \frac{\delta_w}{n\pi}\left[\cos\left(\frac{2n\pi l_w}{\lambda}\right) - 1\right] + \frac{\delta_S - \delta_P}{l_F}$$

$$\times\left\{\frac{\lambda}{2(n\pi)^2}\left[\sin\left(\frac{2n\pi l_S}{\lambda}\right)-\sin\left(\frac{2n\pi l_w}{\lambda}\right)\right]\right.$$
$$\left.-\frac{1}{n\pi}\left[(l_w+l_F)\cos\left(\frac{2n\pi l_S}{\lambda}\right)-l_w\cos\left(\frac{2n\pi l_w}{\lambda}\right)\right]\right\}$$
$$-\frac{\delta_P l_w/l_F(\delta_S-\delta_P)}{n\pi}\left[\cos\left(\frac{2n\pi l_S}{\lambda}\right)\cos\left(\frac{2n\pi l_w}{\lambda}\right)\right] \quad \text{(A3)}$$

References

Aragaki, T., Nakayama, S., Suzuki, M. and Toyama, S. 1987. Characteristics of a falling film on a vertical tube. *Int. Chem. Eng.*, **27**, 326–333

Bach, P. and Villadsen, J. 1984. Simulation of the vertical flow of a thin wavy film using a finite-element method. *Int. J. Heat Mass Transfer*, **27**, 815–827

Barrdahl, R. 1986. On the stability of falling films — Periodic, finite-amplitude waves. *AIChE J.*, **32**, 789–797

Brauner, N. 1989. Modeling of wavy flow in turbulent free falling films. *Int. J. Multiphase Flow*, **15**, 505–520

Chang, H. C. 1987. Evolution of non-linear waves on vertically falling films — A normal form analysis. *Chem. Eng. Sci.*, **42**, 515–533

Grossman, G. 1984. Heat and mass transfer in film absorption. In *The Handbook for Heat and Mass Transfer Operations*, N. P. Cheremisinoff (ed.), Gulf

Kapitza, P. L. 1948. Wave motion of thin viscous layers of liquid — I; Free motion. *J. Exp. Theoret. Phys.* (U.S.S.R.), **18**, 3–18

Karapantsios, T. D. and Karabelas, A. J. 1990. Surface characteristics of roll waves on free falling films. *Int. J. Multiphase Flow*, **16**, 835–852

Kheshgi, H. S. and Scriven, L. E. 1987. Disturbed film flow on a vertical plate. *Phys. Fluids*, **30**, 990–997

Levich, V. G. 1962. *Physicochemical Hydrodynamics*, Prentice-Hall, Englewood Cliffs, NJ, ch. XII

Massot, C., Irani, F. and Lightfoot, E. N. 1966. Modified description of wave motion in a falling film. *AIChE J.*, **12**, 445–455

Miller, W. A. 1992. Experimental and analytical study of aqueous LiBr falling film absorption, Ph.D. diss. proposal, University of Tennessee, USA

Miller, W. A., Perez-Blanco, H. and Patnaik, V. 1992. Advanced surfaces for vertical tube absorbers. Final report to the Gas Research Institute, Contract # 5089-243-1844

Oran Brigham, E. 1974. *The Fast Fourier Transform*, Prentice-Hall, Englewood Cliffs, NJ, Chs. 5 and 6

Patnaik, V. 1994. Combined heat and mass transfer in wavy film absorption. Ph.D. thesis, The Pennsylvania State University, University Park, PA, USA

Patnaik, V., Perez-Blanco, H. and Ryan, W. A. 1993. A simple model for the design of vertical tube absorbers. *ASHRAE Trans.*, **99**

Penev, V., Krylov, V. S., Boyadjiev, C. and Vorotilin, V. P. 1972. Wavy flow of thin liquid films. *Int. J. Heat Mass Transfer*, **15**, 1395–1406

Ruckenstein, E. and Berbente, C. 1965. Mass Transfer in Wave Flow. *Chem. Eng. Sci.*, **20**, 795–801

Seban, R. A. 1978. Transport to falling films, In *Proceedings of the 6th Int. Heat Transfer Conference*, (Toronto, Aug. 7–11), Hemisphere, Bristol, PA, 417–428

Tailby, S. R. and Portalski, S. 1960. The hydrodynamics of liquid films flowing on a vertical surface. *Trans. Inst. Chem. Engrs.*, **38**, 324–330

Uemura, T. and Hasaba, S. 1964. Studies on the lithium bromide-water absorption refrigerating machine. *Tech. Rept. Kansai University*, 6, 31–55

Wasden, F. K. and Dukler, A. E. 1989. Insights into the hydrodynamics of free falling wavy films. *AIChE J.*, **35**, 187–195

Wasden, F. K. and Dukler, A. E. 1990. A numerical study of mass transfer in free falling wavy films. *AICHE J.*, **36**, 1379–1390